Quadrature-Phase-Shift-Keying Direct Modulator Based on Spoof Surface-Plasmon Polaritons

Fei Yang,* Zhi Yu Bi, Han Zhang, Zhan Yi Fu, Chen Xi Liu, Xiao Jian Fu, Jun Wei Wu, and Hui Feng Ma

State Key Laboratory of Millimeter waves, Southeast University, Nanjing 210096, China

(Received 20 April 2023; revised 21 June 2023; accepted 26 June 2023; published 21 July 2023)

The growing demand for ultrafast information transmission in integrated sensing and communications has fueled extensive research on spoof surface-plasmon polaritons (SSPPs). However, existing studies have been limited by structural design constraints, resulting in single-frequency phase modulation and hindered high-order modulation capabilities. Here, we propose a superthin programmable modulator utilizing SSPP waveguides and validate its performance through experimental verification. Our modulator enables phase control across a wider bandwidth by real-time manipulation of SSPP waveguides in a programmable manner, facilitating quadrature-phase-shift-keying modulation. Moreover, this modulator opens up possibilities for achieving higher-order modulation. Measurement results demonstrate the effectiveness of programmable plasma metamaterials in modulating surface electromagnetic waves, with significant implications for integrated sensing and communications applications.

DOI: 10.1103/PhysRevApplied.20.014049

I. INTRODUCTION

Integrated sensing and communications (ISAC) is a rapidly emerging development trend with data modulation serving as a crucial component. Traditional modulation techniques involve the modulation of data onto an intermediate-frequency signal, followed by upconversion to the desired frequency [1]. Although these methods are well established, they require frequency conversion, which adds complexity to the system. Alternatively, direct modulation enables the loading of information onto the carrier signal by directly modulating the amplitude and phase of the rf signal in the transmission path. This approach offers a system with low complexity, simple structure, and reduced power consumption. Consequently, direct modulation provides undeniable advantages in simplifying communication systems for ISAC applications.

Surface-plasmon polaritons (SPPs) are highly localized surface waves that propagate along the interface between materials with positive and negative dielectric constants. The electromagnetic energy of SPP waves is confined within a deep subwavelength range and exponentially decays in the direction perpendicular to the interface [2]. However, at microwave frequencies, metals behave as perfect conductors rather than exhibiting negative dielectric constants as plasmas. To address this challenge, the concept of SSPPs has been introduced, which mimics the behavior of natural SPPs by incorporating a periodic array of subwavelength grooves, holes, or lines on the surface of metals [3,4]. The unique field confinement and enhancement properties of SPP materials offer significant applications in device miniaturization [5,6], low-cross-talk waveguides [7–9], and other related areas [10–16]. Nonetheless, traditional SPPs face limitations in terms of fixed structures and inherent analog properties, making it challenging to achieve dynamic control and establish connections with direct modulation techniques.

To address the challenges of dynamic control in traditional SPP systems, digital technology has been harnessed to control spoof surface-plasmon polaritons (SSPPs) [17–19]. Zhang, Luo, and Cui pioneered the concept of digital SSPP, utilizing a *p-i-n* diode as a state-changing medium to modify the effective tooth height of SSPP units, thereby altering their dispersion state. This innovation opened up possibilities for two-amplitude-shift-keying (2ASK) and two-phase-shift-keying (2PSK) modulation with two shift keys. Subsequently, Zhang *et al*. introduced through holes in the outermost SSPP teeth, transforming the entire waveguide into a bandpass state and enabling a range of modulations, such as 2ASK, 2PSK, and two-frequency-shift-keying [20]. Building upon these advancements, this paper introduces an interdigital capacitance structure into the SSPP waveguide, enabling independent control of SSPP branches and achieving scalable 2-bit modulation capabilities. Here, we present a comprehensive theoretical analysis of the proposed switchable SSPP unit, leveraging the modulation theory of SSPPs. Furthermore, we design a digital phase shifter based on SSPP theory, capable of

*yangfei@seu.edu.cn

 © 2023 American Physical Society

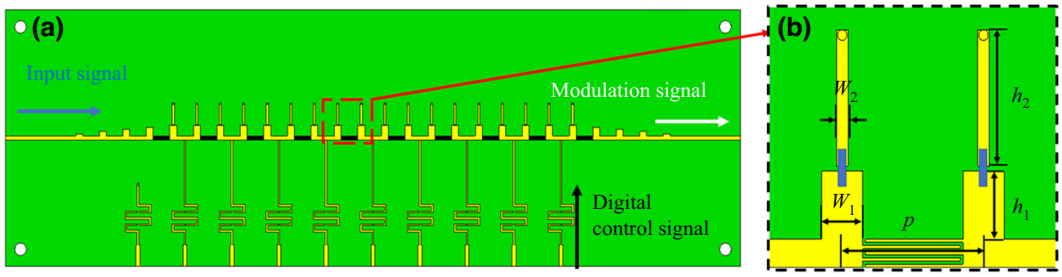

FIG. 1. Proposed SSPP structure. (a) QPSK modulation SSPP waveguide. (b) Schematic diagram of a single switchable SSPP unit, in which period is $p = 6$ mm, radius of the metal hole is $r = 0.2$ mm, widths of metallic bars are $w_1 = 1.75$ mm and $w_2 = 0.5$ mm, heights of metallic bars are $h_1 = 2.5$ mm and $h_2 = 5$ mm, and substrate material is Rogers 4350B.

achieving a phase step of 30° and a total phase shift of 270°. Utilizing this digital phase shifter, we successfully realize direct quadrature-phase-shift-keying (QPSK) modulation. Moreover, to demonstrate the scalability of this QPSK direct modulator, we implement high-order modulation using 16-quadrature-amplitude modulation (QAM). Through theoretical analysis and experimental validation, we establish the effectiveness and versatility of the proposed switchable SSPP unit for enabling direct QPSK and high-order modulation.

II. SSPP MODULATION THEORY

To achieve direct QPSK modulation within a single SSPP unit, a dedicated SSPP structure needs to be carefully designed. The SSPP unit, as depicted in Fig. 1(b), consists of two branches composed of unconnected short stubs, which are interconnected through a *p-i-n* diode at the center. The top short stubs are connected to the bottom metal ground through a via, and the two branches are linked through an interdigital capacitance structure, enabling independent control of the *p-i-n* diodes.

To realize direct QPSK modulation, it is necessary to achieve two distinct transmission states by controlling the *on* or *off* status of the diodes. To elucidate the working principle, a circuit topology is employed, as illustrated in Fig. 2. The two states of a single SSPP unit can be modeled as two circuit structures: the "*on*" state, characterized by a short circuit with an added inductance, and the "*off* " state, characterized by an open circuit with an added capacitance. The main transmission line is considered as a microstrip line with transmission constant k_{m1} and impedance Z_{m1}, while the branching path is represented by conductance Y for Bloch waves propagating in periodic structures [21]. The dispersion formula can be expressed as

$$\cos(kp) = \cos(k_{m1}p) + j\frac{Z_{m1}Y}{2}\sin(k_{m1}p). \tag{1}$$

When the SSPP unit is in the *on* state, it corresponds to a short-circuit configuration, as depicted in Fig. 2(a). In this state, the loaded characteristic impedance can be represented by inductance L, and the corresponding parallel admittance Y can be derived as follows:

$$\begin{aligned} Y_{\text{short}} &= \frac{1}{j\omega L} + \frac{1}{j\omega C_1} + \frac{1}{j\omega L}, \\ &= \frac{2}{jZ_{m2}\tan(k_{m2}h)} + \frac{1}{j\omega C_1}, \end{aligned} \tag{2}$$

in which k_{m2} and Z_{m2} are the wave number and impedance of the reduced shunt branch, respectively. When the SSPP unit is in the *off* state, the designed unit structure is an open circuit, as shown in Fig. 2(b), and the loading characteristic impedance is capacitance C, which can be pushed to its parallel admittance Y as

$$\begin{aligned} Y_{\text{open}} &= j\omega C + j\omega C_1 + j\omega C, \\ &= \frac{2j}{Z_{m2}\cot(k_{m2}h_2)} + j\omega C_1. \end{aligned} \tag{3}$$

By substituting Eqs. (2) and (3) into Eq. (1), capacitance value $C1$ of the interdigital capacitance can be calculated. To obtain the required parameters, we utilize and advanced design system (Keysight) to extract the S parameters. With these extracted parameters, the dispersion curve is calculated, as illustrated in Fig. 3.

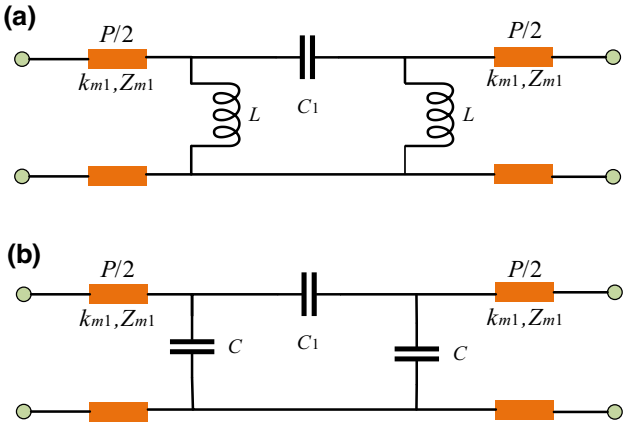

FIG. 2. Equivalent circuit models of the proposed SSPP unit with (a) short-circuit stub and (b) open-circuit stub.

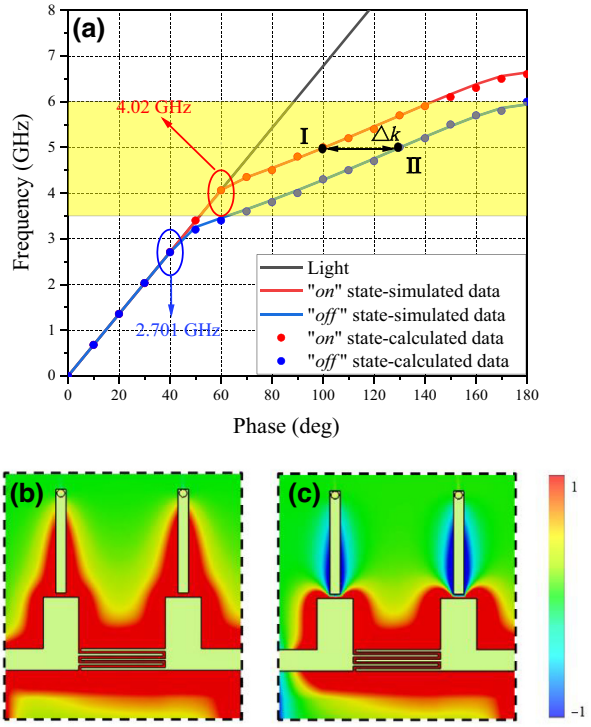

FIG. 3. (a) Dispersion curves of the proposed SSPP unit in the *on* and *off* states. (b),(c) Eigenmode field distributions of the SSPP units in the *on* and *off* states at 5 GHz.

Although the working principle has been described using the circuit model, a quantitative relationship between the circuit parameters and structural parameters has not been established. To determine the structural parameters, the eigenmode analysis can be employed to simulate the SSPP unit depicted in Fig. 1(b). Finite-element analysis is employed to analyze the eigenmode, resulting in dispersion curves for the *on* and *off* states, as depicted in Fig. 3. In the simulation, the *on* state of the *p-i-n* diode is treated as a metal state, while the *off* state is considered as a material with a high relative dielectric constant. The blue and red lines in Fig. 3 represent the dispersion curves for the *on* and *off* states, respectively, which align with theoretical calculations.

Given the flexibility of the proposed structure for designing the SSPP performance by adjusting various parameters, the operating frequency can be customized as desired. For example, modifying the height of the branches allows for frequency tuning. Through careful parameter design, the two dispersion curves can achieve digital phase shifts at specific frequencies, enabling direct QPSK modulation. In Fig. 3(a), points I and II represent states that support SSPP signal transmission with different phase responses. Here, phase refers to the phase shift experienced by the wave as it propagates through the medium at different frequencies. The designed unit structure exhibits a phase difference (Δk) of 30° between different states. By configuring three units to the same state and introducing a phase difference of 90° between four groups of structures, an SSPP waveguide with nine unit structures can achieve four phase shifts of 90°, ensuring stable amplitude and enabling direct QPSK modulation.

From a physical perspective, the switchable state of a *p-i-n* diode is fundamentally related to the control of current flow between the upper and lower metal contacts. In essence, the reconfigurable physical structure enables an adjustable physical response. When the *p-i-n* diode is in the *on* state, as depicted in Fig. 3(b), electromagnetic energy is transmitted through the diode towards the upper metal structure. Low-frequency electromagnetic waves propagate through the metal via holes towards the metal ground plane. This behavior gives rise to the appearance of the dispersion curve with an *on*-state cutoff frequency. The presence of the metal groove structure induces an inductive effect, resulting in the blocking of higher-frequency electromagnetic energy outside the metal ground region, while still supporting the transmission mode of spoof surface-plasmon polaritons.

Conversely, when the *p-i-n* diode is in the *off* state, as shown in Fig. 3(c), electromagnetic energy is prohibited from entering the upper metal contact. Consequently, the dispersion curve exhibits a characteristic low-pass behavior, where higher-frequency components are attenuated.

III. REALIZATION OF THE MODULATION SCHEME

The proposed switchable SSPP unit presents an opportunity to achieve direct communication modulation of QPSK using a single structure. However, discrete physical responses necessitate not only internal structural modifications but also external signal control. Motivated by this concept, a multimode-modulating SSPP waveguide is introduced, where SSPP units with a periodicity of P are arranged along the X axis on a dielectric substrate made of Rogers 4350B. The waveguide is grounded at the bottom metal, as depicted in Fig. 4.

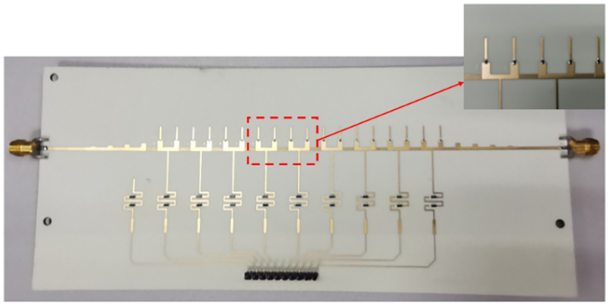

FIG. 4. Photographs of the fabricated prototype.

To enable switching between the *on* and *off* states, the *p-i-n* diode MADP-000907-14020w is selected, and different dc bias voltages are applied between the two ends of the *p-i-n* diode. To prevent high-frequency leakage into the bias network and metal ground, a choke structure comprising meanders and lumped inductors is designed.

Furthermore, two momentum compensations are incorporated to mitigate the mismatch between quasitransverse electromagnetic (EM) modes and SSPP modes. This is achieved by employing a planar gradient refractive-index structure, which helps reduce any discrepancies between the two modes.

To validate the performance of the proposed SSPP waveguide, the transmission spectrum is experimentally measured using a vector network analyzer, and the results are presented in Fig. 5. The measured *S*-parameter results depicted in Fig. 5(a) indicate that, in region I, the amplitudes of the four different states exhibit remarkable similarity, suggesting that all states support the transmission of EM signals. However, their phase responses differ significantly. The inherent variation in wave number between the two states of the *p-i-n* diode switch accumulates along the propagation direction. As illustrated in Fig. 5(b), this accumulation results in a phase difference of 90° between the four states. This characteristic lays the foundation for the implementation of QPSK modulation.

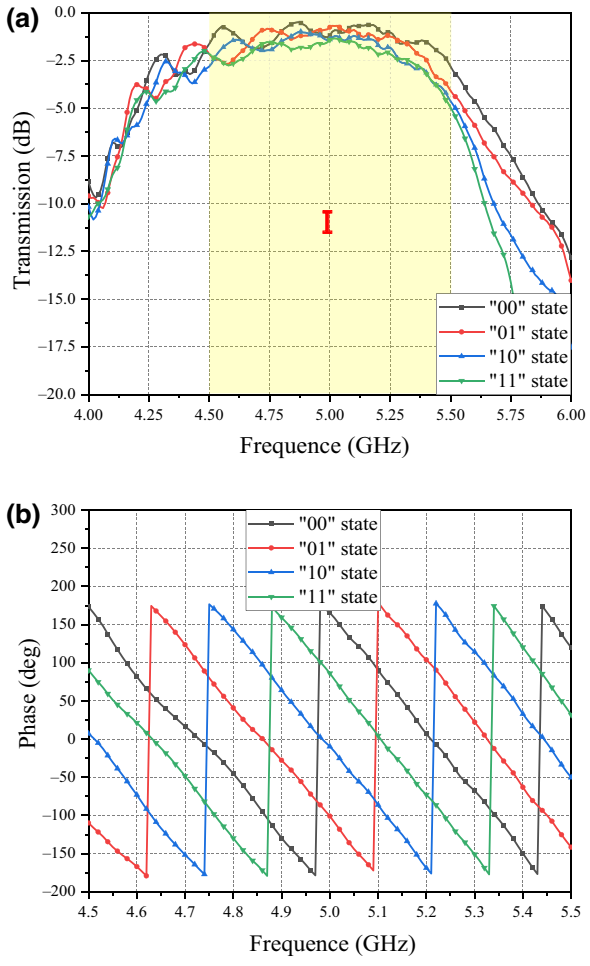

FIG. 5. Measured transmission amplitude (a) and phase spectra (b) of the proposed SSPP waveguide in the "00," "01," "10," and "11" states.

IV. EXPERIMENTAL VERIFICATION OF QPSK MODULATION

Through an analysis of the transmission spectrum, we evaluate the potential of the proposed SSPP waveguide for manipulating EM signals in QPSK modulation. However, the ultimate goal of signal manipulation is to generate modulated signals. Hence, we proceed to demonstrate and verify the performance of the SSPP signal modulated by control signals generated by a field-programmable gate array (FPGA). The experimental system and measurement setup are described in Fig. 6.

To intuitively assess the modulation capability of the proposed SSPP waveguide, we implement direct QPSK modulation. Figure 7(a) illustrates the QPSK modulation signal, which carries 2 bits of phase information (00, 01, 10, and 11). The carrier and modulation frequencies are set to 5 GHz and 1 Msym s^{-1}, respectively. In the constellation diagram, the symbols representing the phase information of QPSK modulation should lie on a circle centered at the origin of the coordinate system. The amplitude of each symbol is roughly the same, and the phase difference between any two states is 90°.

Observing the received constellation in Fig. 7, it can be seen that each symbol is located at its corresponding position on the constellation, aligning with the standard constellation. The measured transmission parameters and phase confirm that QPSK modulation can be achieved across a broad range of carrier frequencies from 4.5 to 5.5 GHz, demonstrating the broadband characteristics of the system.

As the transmission power gradually increases, the constellation diagram becomes denser, indicating a higher bit-error rate, as depicted in Figs. 8(a)–8(d). However, the

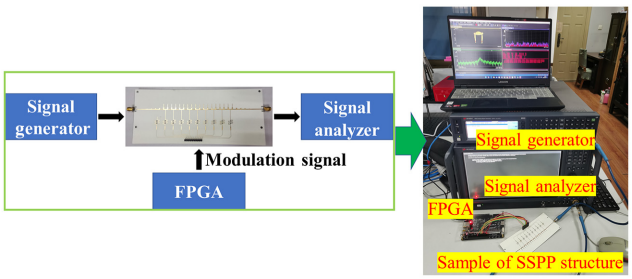

FIG. 6. Schematic diagram of experiment and photograph of experimental setup.

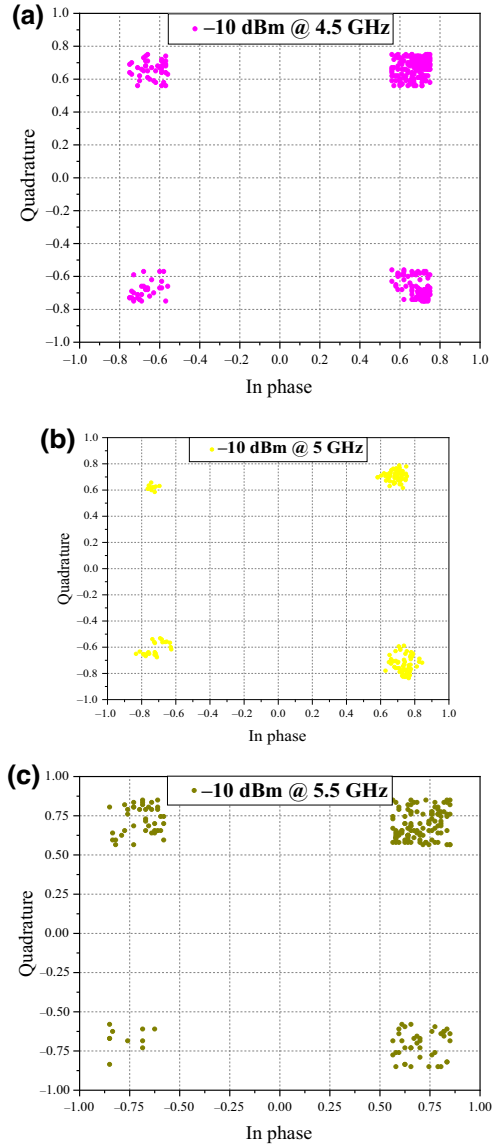

FIG. 7. Measured constellation diagrams. (a) QPSK modulation at a carrier frequency of 4.5 GHz. (b) QPSK modulation at a carrier frequency of 5 GHz. (c) QPSK modulation at a carrier frequency of 5.5 GHz.

proposed SSPP system maintains reliable operation even at a transmission power of −30 dBm.

Furthermore, by keeping the incident intensity constant at −10 dBm and increasing the modulation rate from 1 to 10 Msym s^{-1}, the information symbols can still be successfully distinguished, as demonstrated in Figs. 9(a)–9(c). The measured constellation diagram closely matches the standard constellation diagram, highlighting the system's ability to effectively handle higher modulation rates.

These experimental results validate the robustness and performance of the proposed SSPP system, indicating its suitability for high-speed and reliable communication applications.

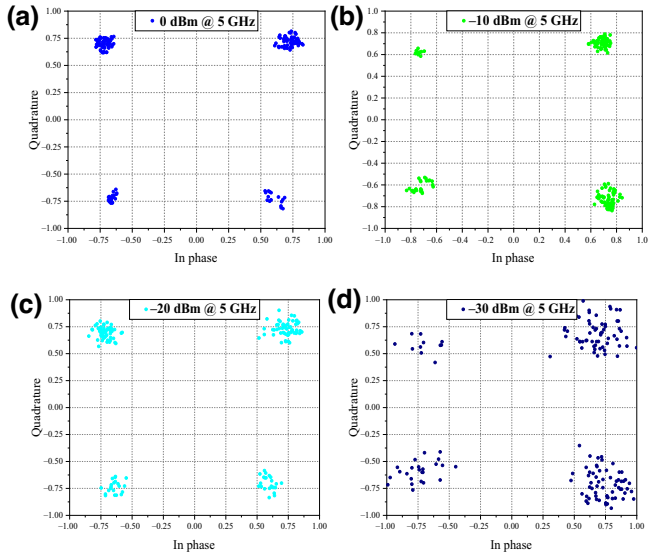

FIG. 8. Measured constellation diagrams. (a)–(d) QPSK schemes with incident intensities of 0, −10, −20, and −30 dBm, respectively, when the modulation rate is 1 MHz.

V. EXPERIMENTAL VERIFICATION OF 16QAM MODULATION

In the context of direct modulation, the technique employed for QPSK can be expanded to achieve 16QAM by modulating the amplitude through two phase shifters. To ensure consistent phase alignment for encoding and transmission, our design incorporates two identical digital phase shifters and a fixed attenuator at the front end. Figure 10 illustrates the specific signal-transmission process.

Initially, the carrier signal is split into two paths using a power splitter. These paths are then connected to the two digital phase shifters, where encoding processing takes place. To create a specific amplitude difference, the amplitude of the signals is subsequently attenuated or amplified. Finally, the two signals are combined using a power combiner, resulting in a 16QAM-modulated signal.

To ensure precise phase alignment, the parameters of the two digital phase shifters are set identically in our design. Additionally, the incorporation of a fixed attenuator at the front end allows for the adjustment of signal amplitude, which contributes to the transmission of 16QAM-modulated signals. This design enhances the efficiency and reliability of signal transmission, facilitating improved performance in 16QAM communication systems.

At a carrier frequency of 5.25 GHz, an input power of −10 dBm, and a modulation rate of 1 Msym s^{-1}, Fig. 11 illustrates the constellation diagram, which demonstrates a low bit-error rate, meeting the requirements of communication.

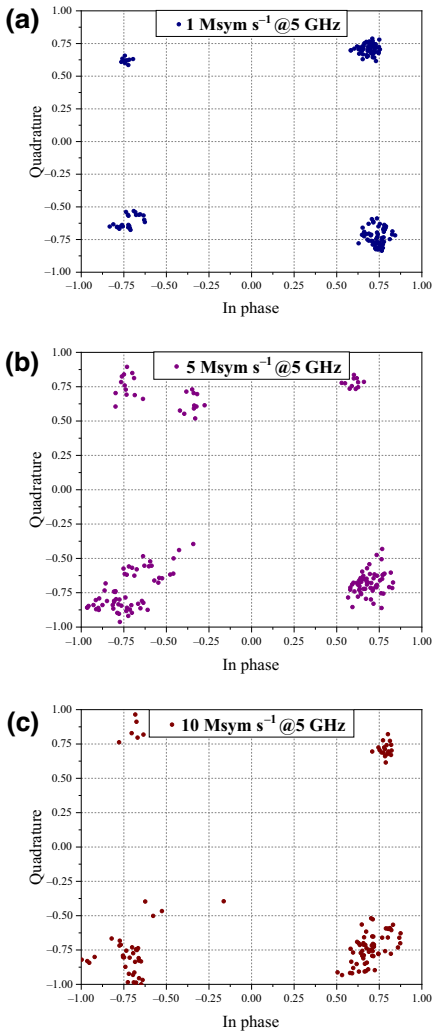

FIG. 9. Measured constellation diagrams. (a)–(c) QPSK schemes with modulation rates of 1, 5, and 10 Msym s^{-1}, respectively, when the input intensity is −10 dBm.

The modulator developed in this study demonstrates a broad communication bandwidth and enables the implementation of QPSK modulation. Moreover, it possesses the potential for further expansion to achieve higher-order modulation schemes. This advancement opens up different possibilities for integrating sensing and communication systems, offering exciting prospects for future applications.

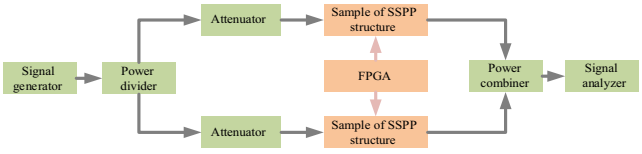

FIG. 10. Transmission process of 16QAM modulation signal.

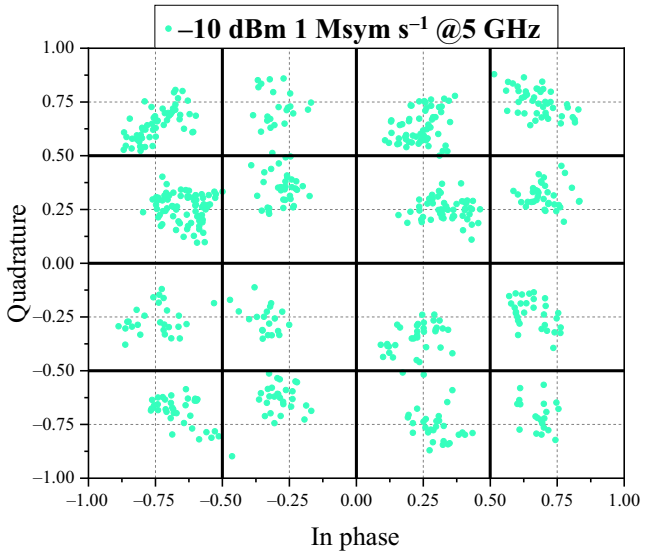

FIG. 11. Measured 16QAM constellation diagram.

VI. CONCLUSION

Our research introduces a pioneering programmable modulator that leverages SSPPs to enable QPSK modulation in wireless communication systems. Through comprehensive experimental investigations, we successfully demonstrate the ability to modulate the phase of the SSPP signal on an extremely thin planar surface. By employing real-time switching of *p-i-n* diodes, we achieve QPSK modulation, and this methodology can be further extended to support higher-order modulation schemes, such as 16QAM.

We anticipate that our study will greatly expand the application of spoof surface-plasmon polariton metamaterials, opening alternative avenues for their utilization in communication engineering. By enabling reliable data-transmission processes with enhanced signal integrity, our work contributes to the advancement of communication technologies.

ACKNOWLEDGMENTS

This work was supported in part by the National Natural Science Foundation of China (Grants No. 12173008 and No. 62071117), the National Key R&D Program of China (Grants No. 2018YFF0109302 and No. 2018YFB1801505), and the Aeronautical Science Foundation of China (Grant No. 201920069002), and in part by the Foundation of Science and Technology on Monolithic Integrated Circuits and Modules Laboratory (Grant No. 614280302032105).

[1] H. Kwakernaak and R. Sivan, Modern signals and systems, NASA STI/Recon Tech. Rep. A **91**, 11586 (1991).

[2] S. A. Maier, *Plasmonics: Fundamentals and Applications* (Springer, New York, 2007).
[3] J. B. Pendry, L. Martín-Moreno, and F. J. Garcia-Vidal, Mimicking surface plasmons with structured surfaces, Science **305**, 847 (2004).
[4] A. P. Hibbins, B. R. Evans, and J. R. Sambles, Experimental verification of designer surface plasmons, Science **308**, 670 (2005).
[5] A. V. Kabashin, P. Evans, S. Pastkovsky, W. Hendren, G. A. Wurtz, R. Atkinson, R. Pollard, V. A. Podolskiy, and A. V. Zayats, Plasmonic nanorod metamaterials for biosensing, Nat. Mater. **8**, 867 (2009).
[6] A. Kianinejad, Z. N. Chen, and C.-W. Qiu, Low-loss spoof surface plasmon slow-wave transmission lines with compact transition and high isolation, IEEE Trans. Microwave Theory Tech. **64**, 3078 (2016).
[7] H. C. Zhang, S. Liu, X. Shen, L. H. Chen, L. Li, and T. J. Cui, Broadband amplification of spoof surface plasmon polaritons at microwave frequencies: Amplification of spoof surface plasmon polaritons, Laser Photonics Rev. **9**, 83 (2015).
[8] W. X. Tang, H. C. Zhang, H. F. Ma, W. X. Jiang, and T. J. Cui, Concept, theory, design, and applications of spoof surface plasmon polaritons at microwave frequencies, Adv. Opt. Mater. **7**, 1800421 (2019).
[9] Y. Bian and Q. Gong, Highly confined guiding of low-loss plasmon waves in hybrid metal-dielectric slot waveguides, Nanotechnology **25**, 345201 (2014).
[10] N. Yu, Q. J. Wang, M. A. Kats, J. A. Fan, S. P. Khanna, L. Li, A. G. Davies, E. H. Linfield, and F. Capasso, Designer spoof surface plasmon structures collimate terahertz laser beams, Nat. Mater. **9**, 730 (2010).
[11] Z. Gao, L. Wu, F. Gao, Y. Luo, and B. Zhang, Spoof plasmonics: From metamaterial concept to topological description, Adv. Mater. **30**, 1706683 (2018).
[12] H. C. Zhang, L. P. Zhang, P. H. He, J. Xu, C. Qian, F. J. Garcia-Vidal, and T. J. Cui, A plasmonic route for the integrated wireless communication of subdiffraction-limited signals, Light: Sci. Appl. **9**, 113 (2020).
[13] H. F. Ma, X. Shen, Q. Cheng, W. X. Jiang, and T. J. Cui, Broadband and high-efficiency conversion from guided waves to spoof surface plasmon polaritons: Broadband and high-efficiency conversion from guided waves to spoof surface plasmon polaritons, Laser Photonics Rev. **8**, 146 (2014).
[14] X. Gao, H. C. Zhang, P. H. He, Z. X. Wang, J. Lu, R. T. Yan, and T. J. Cui, Crosstalk suppression based on mode mismatch between spoof SPP transmission line and microstrip, IEEE Trans. Compon., Packag., Manuf. Technol. **9**, 2267 (2019).
[15] X. Gao, J. Zhang, H. C. Zhang, L. Liu, Q. Ma, P. Xu, and T. J. Cui, Dynamic controls of second-harmonic generations in both forward and backward modes using reconfigurable plasmonic metawaveguide, Adv. Opt. Mater. **8**, 1902058 (2020).
[16] P. Hang He, H. Chi Zhang, X. Gao, L. Yun Niu, W. Xuan Tang, J. Lu, L. Peng Zhang, and T. Jun Cui, A novel spoof surface plasmon polariton structure to reach ultra-strong field confinements, Opto-Electron. Adv. **2**, 19000101 (2019).
[17] H. C. Zhang, T. J. Cui, Y. Luo, J. Zhang, J. Xu, P. H. He, and L. P. Zhang, Active digital spoof plasmonics, Natl. Sci. Rev. **7**, 261 (2020).
[18] X. Gao, W. Y. Cui, Z. Gu, J. Zhang, Y. Ren, Q. Ma, and T. J. Cui, Multimode and reconfigurable phase shifter of spoof surface plasmons, IEEE Trans. Antennas Propagat. **71**, 5361 (2023).
[19] X. Gao, Z. Gu, Q. Ma, W. Y. Cui, T. J. Cui, and C. H. Chan, Reprogrammable spoof plasmonic modulator, Adv. Funct. Mater. **33**, 2212328 (2023).
[20] L. Zhang, H. Zhang, M. Tang, P. He, L. Niu, L. Liu, J. Lu, W. Tang, J. Mao, and T. Cui, Integrated multi-scheme digital modulations of spoof surface plasmon polaritons, Sci. China Inf. Sci. **63**, 202302 (2020).
[21] H. C. Zhang, T. J. Cui, J. Xu, W. Tang, and J. F. Liu, Real-time controls of designer surface plasmon polaritons using programmable plasmonic metamaterial, Adv. Mater. Technol. **2**, 1600202 (2017).